I. Introduction

For the past three years, XTM has been funded under the Advanced Computational Technology Initiative (ACTI). The ACTI program is designed to enhance, apply, and transfer advanced computational technology for finding, developing, and producing natural gas and oil. The ACTI program supports interaction between the DOE National Laboratories and industrial partners in the domestic natural gas and oil industry, with industry providing cost-sharing through in-house efforts or in-kind support. Radiation transport simulation plays a key role in modeling and designing radiation based oil-well logging tools. Under Task 1, XTM was assigned to develop and apply deterministic transport methods to well logging tool design and assess the effectiveness of such methods.

Many applications of radiation transport require accurate modeling of complex three-dimensional geometries, and nuclear oil well logging tools certainly fall into this category. These problems usually involve a complex geometry with fixed sources and one or more detectors. Detector responses must generally be accurate to a few percent. Historically, Monte Carlo codes have been used for modeling oil well logging tools. Existing deterministic transport codes have not been routinely used primarily because of the difficulties of modeling complex geometries with rectangular meshes. Monte Carlo codes are able to handle the complex geomtries, but can suffer from prohibitively long computer times to achieve acceptable statistical accuracy. For a historical review of multidimensional radiation transport techniques used to model radiation based well logging tools refer to Ullo[1].

With partial funding from ACTI, XTM researchers have developed a three-dimensional S_n code, ATTILA[2], which uses linear discontinuous spatial differencing in conjunction with diffusion-synthetic acceleration (DSA) on a unstructured tetrahedral mesh. This tetrahedral mesh capability enables the accurate modeling of complex three dimensional geometries. Various capabilities specifically designed for oil well logging calculations have been added to ATTILA.

This report will focus on the application of ATTILA to oil well logging tools including:

- A general description of ATTILA
- Grid Generation
- Material data (cross sections)
- Results for a neutron porosity tool.
- Results for a gamma ray density tool.

II. The ATTILA Code

ATTILA is a time-independent, scalar (not parallel) three-dimensional transport code designed for neutron, gamma-ray, or electron transport calculations. The main features of ATTILA include:

1. discrete ordinates (S_n) angular discretization
2. unstructured tetrahedral mesh
3. linear discontinuous finite element spatial differencing

4. multigroup energy discretization
5. arbitrary order anisotropic scattering
6. diffusion synthetic acceleration (DSA) of within-group scattering iterations
7. first collision source (for point sources)
8. last collided flux calculation

The unstructured tetrahedral mesh allows for accurate modeling of complex three-dimensional geometries. The linear discontinuous spatial differencing scheme is considerably more accurate than traditional diamond or weighted diamond finite difference

schemes and allows the use of relatively coarse meshes. The use of DSA significantly increases the efficiency of the code. The first collision[3] source helps mitigate ray-effects associated with the S_n method due to singular point sources and is necessary for the gamma-ray density tools. The last collided flux calculation is necessary for accurately determining the detector responses in the near detector of gamma-ray tools.

III. Grid Generation

The ability to generate good unstructured tetrahedral grids (meshes) is very important and a key component to the success of ATTILA on logging problems. Two commercial grid generators have been investigated, GRIDGEN and ICEM.

GRIDGEN, by Pointwise Inc., is a very well-known and widely used grid generator for multi-block hexahedral meshes. Meshes are usually created from a CAD geometry. Recently, with the release of GRIDGEN V13, an unstructured tetrahedral mesh capability has been added. GRIDGEN is relatively easy to learn and use and the user support provided by Pointwise is very good. For now, GRIDGEN cannot generate the tetrahedral meshes for the logging tools, because of the tangential intersection between the tool and the borehole. Pointwise is aware of the problem and hopefully in the near future GRIDGEN will be able to handle these problems.

ICEM, by ICEMCFD Engineering, is a very powerful and widely used grid generator. Both multi-block hexahedral and unstructured tetrahedral meshes can be generated. All meshes are generated from a CAD geometry. In fact, ICEM comes with a full featured CAD package, but commercial CAD packages, such as PROENGINEER, can be used as well. ICEM is not as easy to learn as GRIDGEN, but after a user has become experienced, one can generate grids much faster. ICEM can generate the tetrahedral meshes for the logging tools. A experienced ICEM user can generate both the CAD geometry and tetrahedral mesh for the logging tools in about 2-4 hours, where about 75% of the time is spent in generating the CAD geometry. The user support by ICEMCFD Engineering is very good as well. ICEMCFD Engineering has generated a mesh translator to write an RTT mesh file for defining the grid. The RTT file format was created here in XTM and is used by all of our unstructured grid codes. At this time ICEM is the recommended grid generator for unstructured tetrahedral meshes.

IV. Cross Sections

Cross sections are extremely important for achieving high accuracy on the logging tools. ATTILA uses multigroup cross sections, which can be in DTF, MENDF, or BXSLIB formats. For neutrons, we have investigated both MENDF and BUGLE-80 cross sections. We have found that MENDF cross sections are inadequate. BUGLE-80 cross sections appear to be adequate for the neutron tools as will be shown in Section V. For gamma-rays, we use CEPXS[4] to generate the cross sections. CEPXS is widely used for coupled electron-photon calculations. CEPXS allows for arbitrary group structure and can generate scattering cross section moments up to P_{15}.

V. Neutron Porosity Tool

Dual detector neutron porosity tools commonly measure a ratio of count rates from two detectors that are located at different distances from the source. The ratio is governed mainly by the slowing down length of the formation, which is sensitive to the amount of hydrogen in place. Since hydrogen is usually associated with pore fluids, a calibration of the count rate ratio in terms of porosity is possible.

The specifications for the neutron tool we have modeled with ATTILA are as follows:

- Tool axis off-centered at 6.35 cm from the borehole axis**.**
- Neutron source: ^{241}Am-Be isotropic point source on tool axis located 50 cm above the bottom of the formation.
- Assume that all collisions in the detectors lead to a count.
- Neutron Output = 10^7 neutrons/s.
- Detectors (right circular cylinders):
    - Type-^{3}He filled proportional counters,
    - ^{3}He gas density = 0.503g/liter,
    - Near detector diameter = 2.54 cm,
    - Near detector length = 7.62 cm,
    - Near detector center-to-source distance = 19.05 cm,
    - Far detector diameter = 5.08 cm,
    - Far detector length = 25.4 cm,
    - Far detector center-to-source distance = 50.08 cm.
- Tool (right circular cylinder):
    - Diameter is 7.62 cm,
    - Length = 150 cm,
    - Material is pure iron (7.8 g/cm^3).
- Borehole (right circular cylinder):
    - Diameter is 20.32 cm,
    - Length = 150 cm,
    - Material is fresh water (1.0 g/cm^3).
- Formation (right circular cylinder):
    - Diameter =120 cm,

  - Length = 150 cm,
  - Material = $CaCO_3$ (2.7 g/cm^3),
  - Pore Material = Pure Water (1.0 g/cm^3),
  - Porosity values = 20 PU and 1 PU.
- Solutions:
  - Calculate the count rate in each detector at each porosity value,
  - Calculate the ratio of the near to far detector count rates at each porosity value.

Reference solutions, which are given in Table 1, come from MCNP[5] calculations with continuous energy cross sections. The MCNP calculations used extensive variance reduction techniques and required approximately 10 hours on a SGI Octane with a 250 Mhz R10000 processor.

TABLE 1
MCNP Results for Neutron Porosity Tool

Porosity (PU)	Near Detector Count Rate	Far Detector Count Rate	Ratio Near/Far
1	7.150E+3 (0.51%)	6.619E+3 (0.31%)	1.08 (0.60%)
20	6.430E+3 (0.54%)	1.862E+3 (0.46%)	3.45 (0.96%)

The tetrahedral mesh for this problem is shown in Figure 1. Because of the symmetry about the y-axis, we model one-half of the problem with appropriate symmetry boundary conditions. Vacuum boundaries are used on all non-symmetry boundaries. The mesh was generated with ICEM and consists of 43,012 tetrahedra. The problem was solved using ATTILA both with and without the first collision source option. The scalar fluxes were converged to a relative pointwise convergence of 10^{-3}. Triangular Tchebyshev-Legendre quadrature was used for all calculations. The BUGLE-80 47-group neutron cross section set was used with both P_1 and P_2 diagonal transport corrected scattering. DSA was used on all calculations. All calculations were run on an SGI Octane with a 250 Mhz R10000 processor. Computing times ranged from approximately 2 hours for the S_4-P_1 calculation to 7 hours for the S_8-P_1 calculation. Without DSA the computing times are more than doubled.

Table 2 gives results from ATTILA for the near and far detector count rates and the ratio of the count rates at 1 PU using various S_n orders with and without the first collision source. Here we see that transport corrected P_1 scattering appears to be sufficient. It appears that S_4 quadrature is adequate for angular convergence. We note that the first collision source does not appear to be necessary for these calculations

TABLE 2
ATTILA Count Rates for Neutron Porosity Tool at 1 PU

S_n/P_n Order	First Collision Source (on/off)	Near Detector Count Rate	Far Detector Count Rate	Ratio Near/Far
S_4/P_1	on	7.047E+3	6.372E+3	1.10
S_4/P_2	on	7.032E+3	6.379E+3	1.10
S_4/P_1	off	7.105E+3	6.355E+3	1.12
S_6/P_1	on	7.041E+3	6.404E+3	1.10
S_6/P_1	off	7.10E+3	6.395E+3	1.11
S_8/P_1	on	7.040E+3	6.410E+3	1.10
S_8/P_1	off	7.080E+3	6.401E+3	1.11

Table 3 gives results from ATTILA for near and far detector count rates and the ratio of the count rates at 20 PU using various S_n orders with and without the first collision source. Again, we see that transport corrected P_1 scattering appears to be sufficient. It appears that S_6 or S_8 quadrature is required for angular convergence, depending on the accuracy required. We still see fairly good agreement with the Monte Carlo results. The larger differences between the ATTILA calculations and Monte Carlo possibly arise from the differences between multigroup and continuous energy cross sections. Differences may also arise from spatial error. Again, the first collision source does not appear to be necessary. Computing times are nearly the same as those at 1 PU.

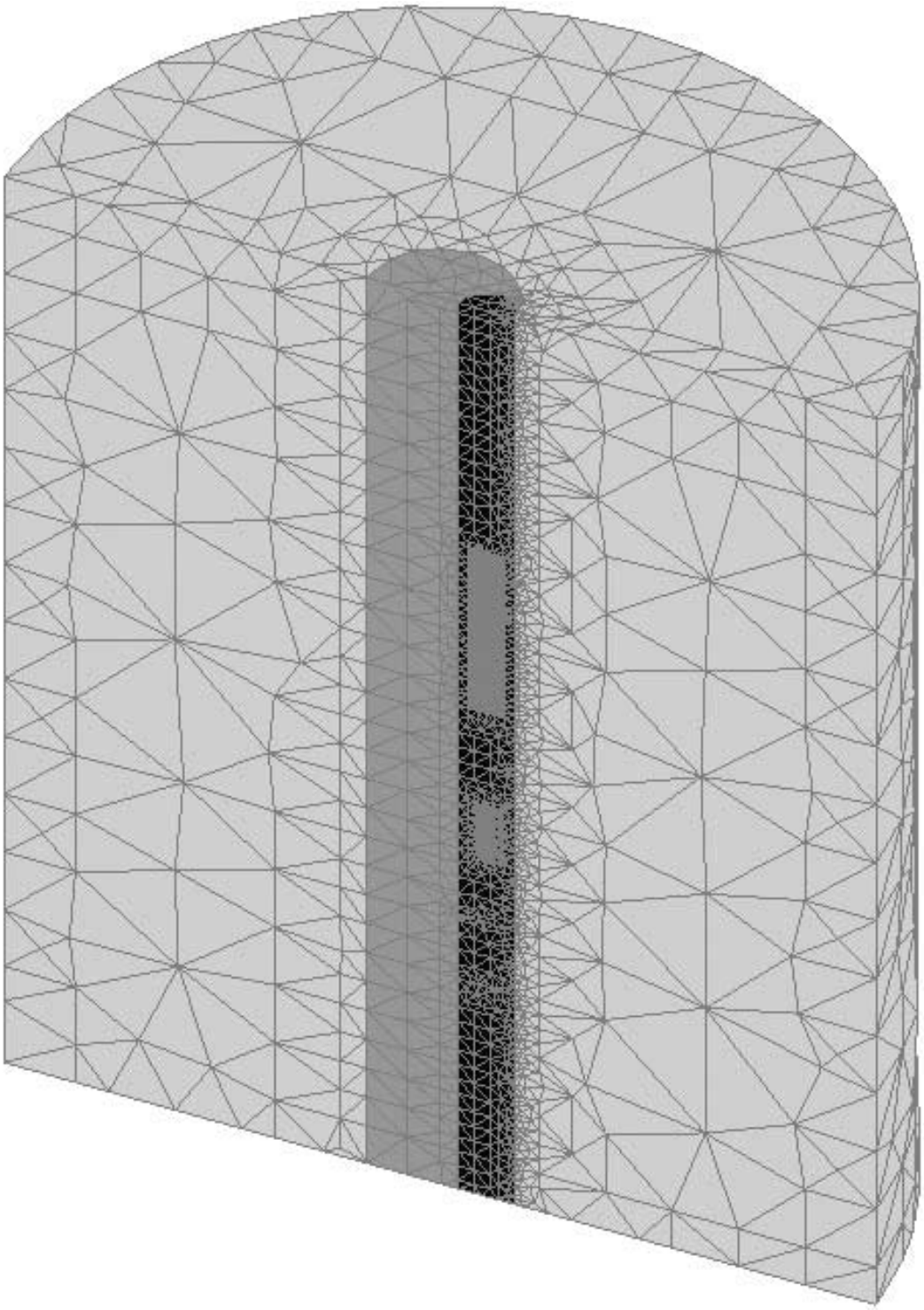

Figure 1: Grid for Neutron Porosity Tool

TABLE 3
ATTILA Results for Neutron Porosity Tool at 20 PU

S_n/P_n Order	First Collision Source (on/off)	Near Detector Count Rate	Far Detector Count Rate	Ratio Near/Far
S_4/P_1	on	6.402E+3	1.879E+3	3.41
S_4/P_2	on	6.376E+3	1.869E+3	3.41
S_4/P_1	off	6.460E+3	1.859E+3	3.47
S_6/P_1	on	6.395E+3	1.912E+3	3.34
S_6/P_1	off	6.455E+3	1.896E+3	3.40
S_8/P_1	on	6.385E+3	1.922E+3	3.32
S_8/P_1	off	6.385E+3	1.887E+3	3.38

VI. Gamma Density Tool

A gamma density logging tool exploits the fact that gamma rays with energies > 200 keV interact with matter mainly through Compton scattering with individual electrons. Since the Compton scattering cross section varies as the electron density of the material, which can be simply related to the bulk density, a measurement of gamma ray intensity can be employed to determine density. Simply stated, the logarithm of the count rates in each of the detectors is proportional to the density. Often times, a layer of mudcake builds up on the borehole, which has a different density than the formation. In this case, it is necessary to use two different detectors to account for the mudcake layer.

A. Without Mudcake

The specifications for the gamma density tool without mudcake are as follows:

- Gamma source: ^{137}Cs isotropic and monoenergetic (0.662 MeV) point source on tool axis located 12.7 cm above the bottom of the formation and 4.92125 cm to the right of the borehole axis.
- Gamma ray Output = 0.74×10^{11} gamma-rays/s.
- Assume that all collisions with energies between (0.55 MeV and 0.15 MeV) in the detectors lead to a count.
- Detectors (right circular cylinders):
    - Material is NaI (3.667 g/cm^3),
    - Near detector diameter = 3.048 cm,
    - Near detector length = 3.81 cm,

- Near detector center-to-source distance = 20.955 cm,
- Near detector center-to-borehole axis = 4.92125 cm,
- Far detector diameter = 5.08 cm,
- Far detector length = 5.08 cm,
- Far detector center-to-source distance = 40.64 cm,
- Far detector center-to-borehole axis = 4.92125 cm.

- Tool is enclosed within a plane at x=-0.15875 cm for the left side; planes at y=5.08 cm and -5.08 cm for the inner and outer sides; planes at z=-12.7 cm and 50.8 cm for the top and bottom sides; and a right circular cylinder with axis at x=2.38125 cm and a radius of 7.62 cm for the right side. Material is pure tungsten (19.2 g/cm^3).
- Borehole (right circular cylinder):
  - Diameter is 20.0025 cm,
  - Length = 50.8 cm,
  - Material is fresh water (1.0 g/cm^3).
- Formation (right circular cylinder):
  - Diameter = 100.0025 cm,
  - Length = 50.8 cm,
  - Material = $CaCO_3$ (2.71 g/cm^3),
  - Pore Material is fresh water (1.0 g/cm^3),
  - Porosity values = 59.06, 29.82 and 0,
  - Density values =1.7 , 2.2 and 2.71 g/cm^3.
- Other Characteristics
  - Source collimator hole is a 1.9047 cm diameter right circular cylinder with axis at +45 degrees in X-Z plane centered on source enclosed with a plane at x=0 on the left and by the tool boundary on the right. Contains nitrogen (22 a/o) and oxygen (78 a/o) at a density of 0.001 g/cm^3.
  - Near detector collimator hole is a 1.27 cm diameter right circular cylinder with axis at -45 degrees in X-Z plane. The axis intersects the near detector 1.016 cm above the bottom of the near detector. The left side intersects the near detector and the right side intersects the tool boundary. Contains nitrogen (22 a/o) and oxygen (78 a/o) at a density of 0.001 g/cm^3.
  - Far detector collimator hole is a rectangular region enclosed by the one half of the far detector on the left and by the tool on the right. The height and width are equal to the diameter of the far detector. Contains nitrogen (22 a/o) and oxygen (78 a/o) at a density of 0.001 g/cm^3.
- Solutions:
  - Calculate the count rate in each detector for all three formation density values,
  - For each detector, calculate the slope, α, of the line given by, $\ln C = C_0 + \alpha\rho$, where C is the count rate and ρ is the density, using the count rates at the three different formation densities.

Reference solutions come from MCNP[5] calculations with continuous energy cross sections. These calculations were obtained using a special version[6] of MCNP, which uses tetrahedral based weight windows for variance reduction. The tetrahedral weight windows were generated using two S_{10}, P_7 ATTILA adjoint calculations with 6 energy groups, one for the far detector and one for the near detector. The first collision source option was used for the near detector adjoint calculation assuming a point source

near the entrance of the near detector through the near detector collimator hole. Speedups of over 100 for the near detector and over 1000 for the far detector were observed using the ATTILA generated weight windows. The calculations required approximated 8 -10 hours for the far detector and approximately 30-40 hours for the near detector. However, to get the near detector results within a error of less than 1% would require over 100 hours. Without biasing, it is doubtful that calculations could have been completed.

The MCNP count rates are given in Table 4 and the slope values are given in Table 5. Here the slopes are calculated using linear regression. We have statistical estimates for the errors in the count rates but do not have statistical estimates for the error in the slopes. We attemt to give some indication of the MCNP error for the slope values where the "maximum and average" values of the error in α are defined by :

$$\Delta\alpha_{\max} = Max\left[\Delta\alpha(C_1 \pm E_1, C_2 \pm E_2, C_3 \pm E_3)\right],$$

$$\Delta\alpha_{av} = \frac{1}{8}\sum\left[\Delta\alpha(C_1 \pm E_1, C_2 \pm E_2, C_3 \pm E_3)\right].$$

These error measures are given in Table 5.

TABLE 4
MCNP Count Rates for Gamma Density Tool Without Mudcake

	Count Rate	
Density (Porosity)	Near Detector	Far Detector
1.7 (59.06)	14062.2 (1.92%)	15398.6 (1.71%)
2.2 (29.82)	11338.3 (1.76%)	5520.0 (1.50%)
2.71 (0)	8713.1 (1.98%)	1878.8 (1.12%)

TABLE 5
MCNP Slopes for Gamma Density Tool Without Mudcake

Detector	α	$\Delta\alpha_{\max}$	$\Delta\alpha_{av}$
Near	-0.473	8.15%	4.82 %
Far	-2.083	1.34%	0.82%

Due to the collimated sources and detectors, gamma-ray density tools present many challenges to deterministic transport codes. To obtain the most accurate solutions, we proceed as follows for each individual calculation:

1. Begin by using the first collision source option.
2. Run a regular S_n calculation. Here the scattering source (expanded in spherical harmonics) is assumed to be good everywhere except the near detector. We also assume that the far detector solutions from the regular S_n calculation are good. The near detector is highly collimated and the S_n method is not expected to do well.

3. Generate a biased quadrature set that has many angles in the solid angle associated with the detector collimator hole. We have a simple procedure for generating these quadrature sets.

4. Using the spherical harmonic moments of the scattering source as a fixed source, use ATTILA with the bias quadrature set to perform a last collided flux calculation into the near detector. This is essentially one inner iteration for each energy group.

The tetrahedral mesh used in ATTILA for this problem is shown in Figure 2. Because of the symmetry, we model one-half the problem with appropriate symmetry boundary conditions. Vacuum boundaries are used on all non-symmetry boundaries. The mesh was generated with ICEM and consists of 35,698 tetrahedra. The scalar fluxes were converged to a relative pointwise convergence of 10^{-2}. Triangular Tchebyshev-Legendre quadrature was used for all calculations. CEPXS cross sections were used with 12 energy groups. The energy group structure is given in Table 6. S_{16} quadrature was used with P_8 scattering. The biased quadrature set contained 288 quadrature directions, with 128 directions in the solid angle associated with the near collimator hole. All calculations were run on an SGI Octane with a 250 Mhz R10000 processor. Computing times are approximately 12 hours.

We have performed some parametric studies, but these have been limited due to memory constraints. We have found that S_{14} quadrature would probably be sufficient for these calculations. Although we have shown the S_{16} results, we find less than 1% difference between the two. We have found that P_8 scattering appears to be sufficient with smaller orders adding too much additional error. Higher order scattering requires too much additional memory at this time. We have not performed a mesh study to determine the errors introduced by spatial error, group structure error, or multigroup cross section error.

The count rates from ATTILA are given in Table 7 and the slopes are given in Table 8. Figure 3 provides a semi-log plot of the count rates from MCNP and ATTILA as a function of density for both detectors.

TABLE 6
Energy Group Structure for Gamma Tools

Group Number	Upper Energy (MeV)	Lower Energy (MeV)
1	0.724	0.60
2	0.60	0.55
3	0.55	0.40
4	0.40	0.35
5	0.35	0.325
6	0.325	0.30
7	0.30	0.275
8	0.275	0.25
9	0.250	0.225
10	0.225	0.20
11	0.20	0.175
12	0.175	0.150

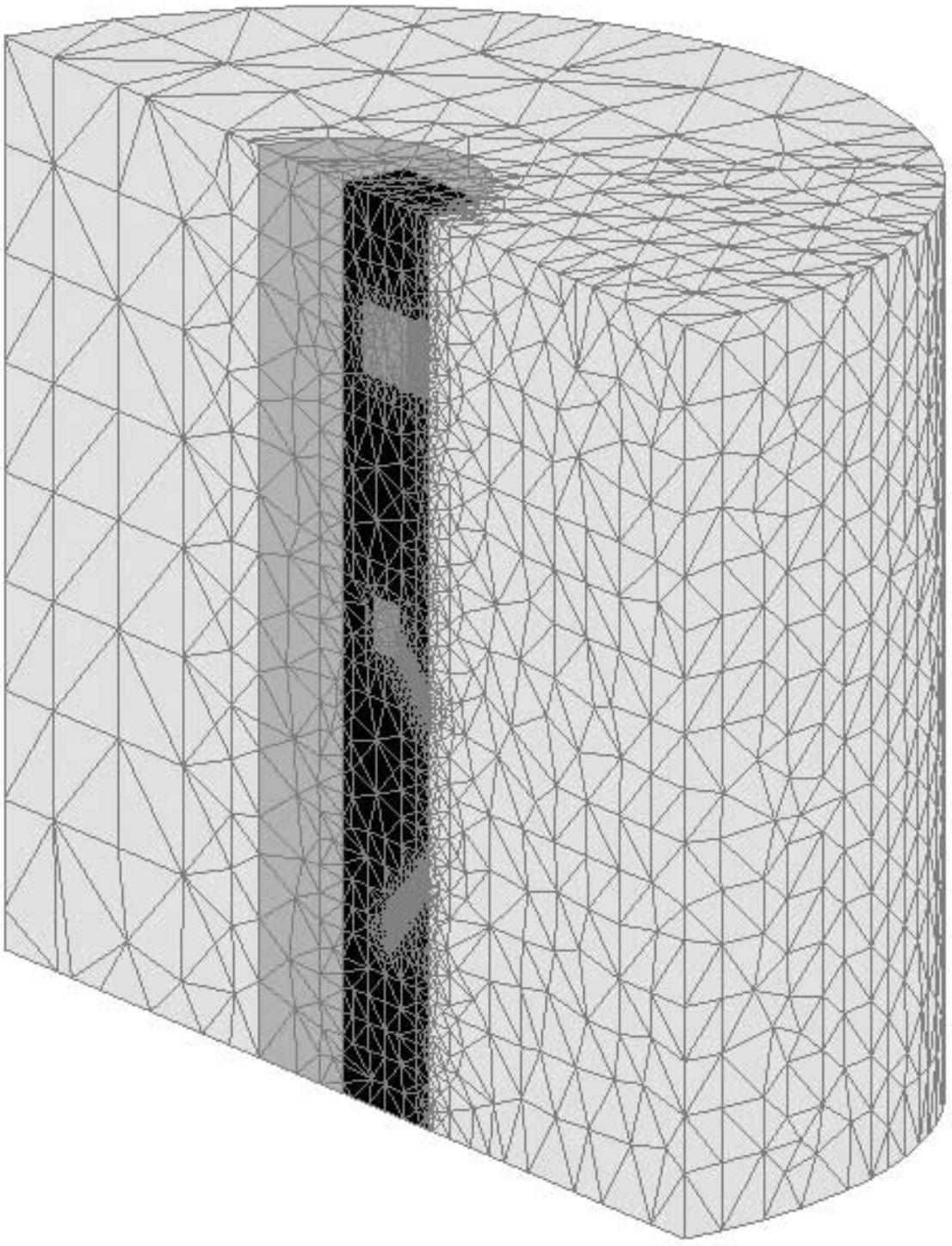

Figure 2: Grid for Gamma Density Tool Without Mudcake

TABLE 7
ATTILA Count Rates for Gamma Density Tool Without Mudcake

	Near Detector	Far Detecor

Density (Porosity)	Count Rate	ATTILA /MCNP	Count Rate	ATTILA /MCNP
1.7 (59.06)	12025.0	0.855	13889.8	0.902
2.2 (29.82)	9738.4	0.860	5080.8	0.920
2.7 (0)	7506.3	0.862	1742.0	0.928

TABLE 8
ATTILA Slopes for Gamma Density Tool Without Mudcake

Detector	α	Difference From MCNP
Near	-0.465	1.70%
Far	-2.0	1.30%

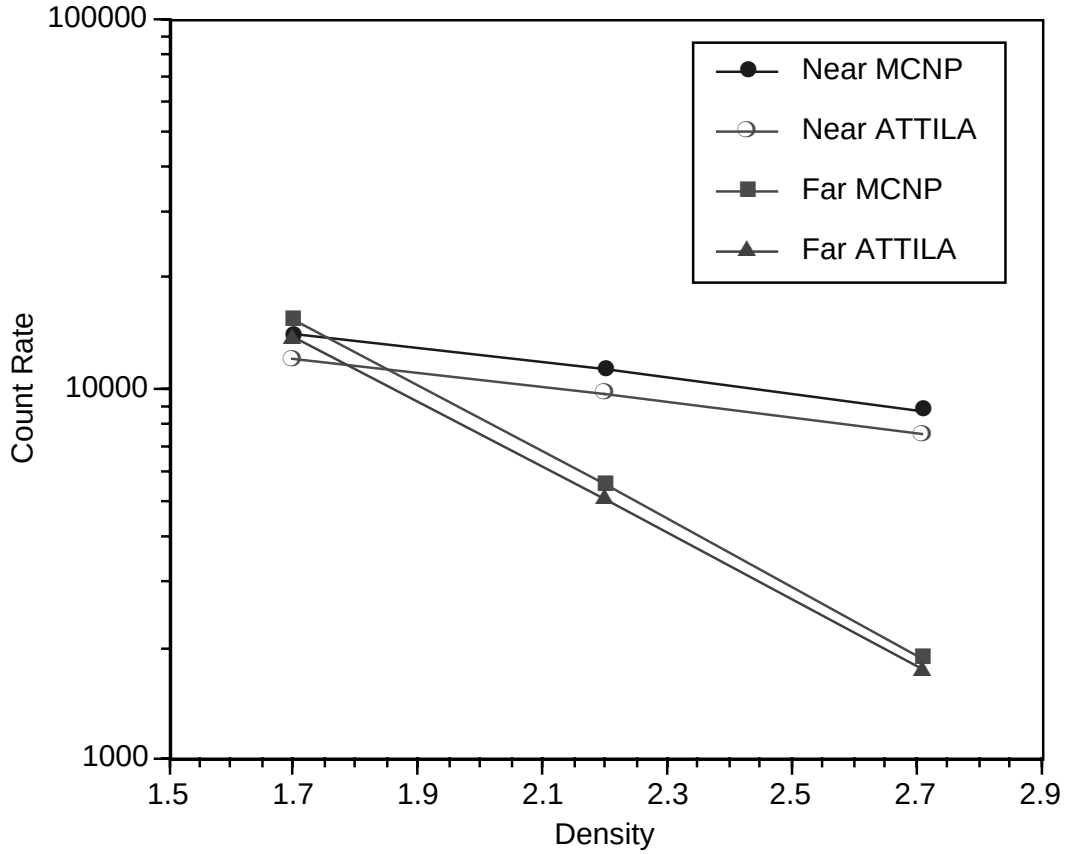

Figure 3: MCNP and ATTILA Count Rates Versus Density
for Gamma Density Tool Without Mudcake

B. With Mudcake

The specifications for the gamma density tool with mudcake are nearly the same as that in the previous section. Here, there is a 0.635 layer of mudcake (right circular cylinder on the surface of the borehole. Therefore, the tool is moved -0.635 cm to the left (-x direction) and the effective borehole diameter is 1.27 cm less than before. The mudcake layer is assumed to have a porosity of 40.95 (density = 1.7 g/cm^3).

Reference solutions come from MCNP calculations with continuous energy cross sections. Run times are nearly the same as those reported for the problem without mudcake. The count rates are given in Table 9 and the slopes are given in Table 10. Again, the special tetrahedral mesh weight window version of MCNP was used.

TABLE 9
MCNP Results for Gamma Density Tool With Mudcake

	Count Rates	
Density (Porosity)	Near Detector	Far Detector
1.7 (59.06)	13732.9 (1.58%)	15170.2 (1.18%)
2.2 (29.82)	11721.6 (1.86%)	5725.4 (1.10%)
2.71 (0)	10055.8 (1.65%)	2079.4 (1.29%)

TABLE 10
MCNP Slopes for Gamma Density Tool Without Mudcake

Detector	α	$\Delta\alpha_{\max}$	$\Delta\alpha_{av}$
Near	-0.309	10.4%	5.35%
Far	-1.968	1.24%	0.65 %

The tetrahedral mesh for this problem is shown in Figure 4. The count rate results from ATTILA, using the same procedure as before, are given in Table 11. The ATTILA slopes are give in Table 12. Figure 5 provides a semi-log plot of the count rates from MCNP and ATTILA as a function of density for both detectors.

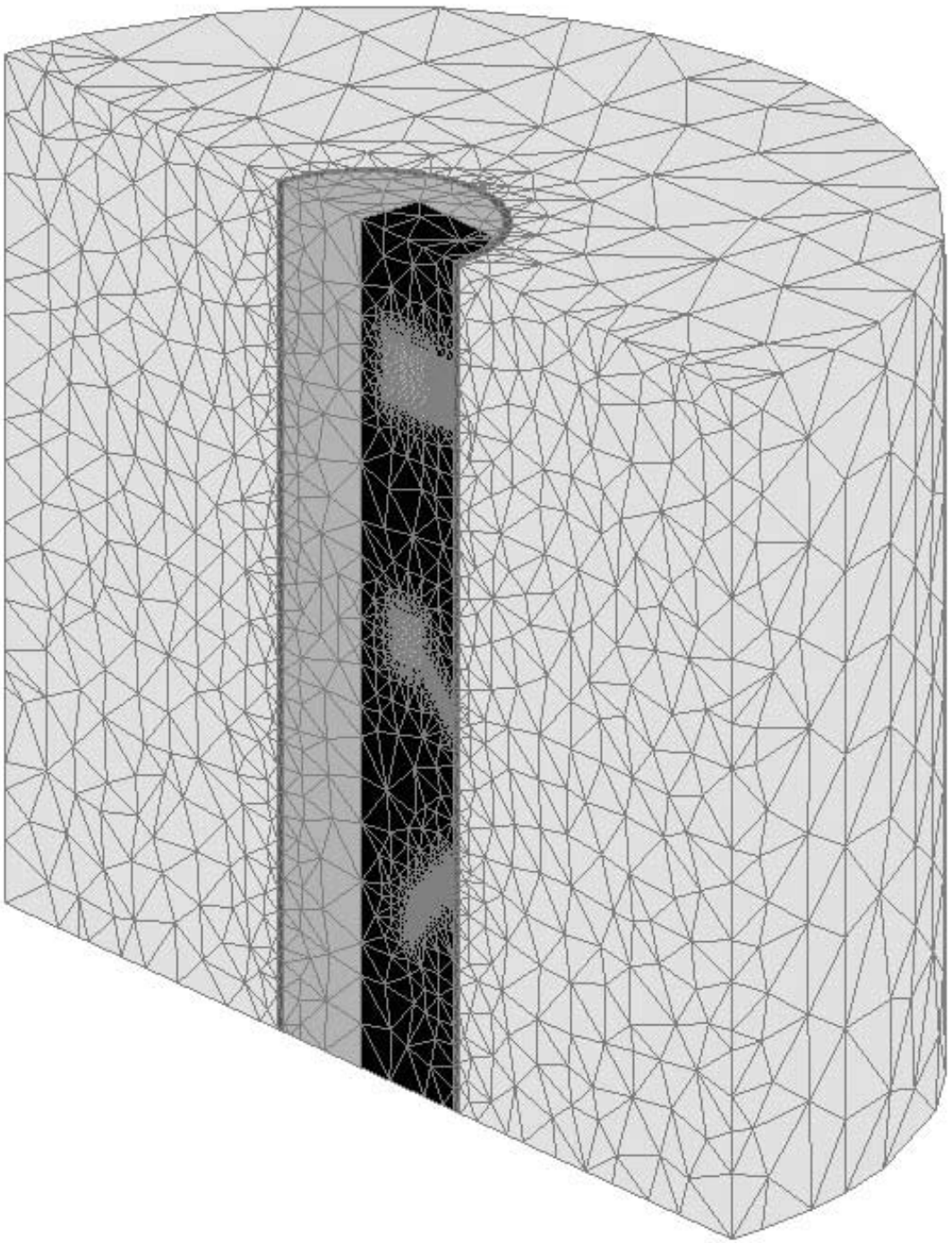

Figure 4: Grid for Gamma Density Tool With Mudcake

TABLE 11
ATTILA Count Rates for Gamma Density Tool With Mudcake

	Near Detector		Far Detecor	
Density (Porosity)	Count Rate	ATTILA /MCNP	Count Rate	ATTILA /MCNP
1.7 (40.94)	11218.4	0.817	14000.8	0.923
2.2 (29.82)	9785.5	0.834	5357.6	0.936
2.7 (0)	8177.0	0.813	1931.4	0.929

TABLE 12
ATTILA Slopes for Gamma Density Tool With Mudcake

Detector	α	Difference From MCNP
Near	0.313	1.28%
Far	1.961	0.36%

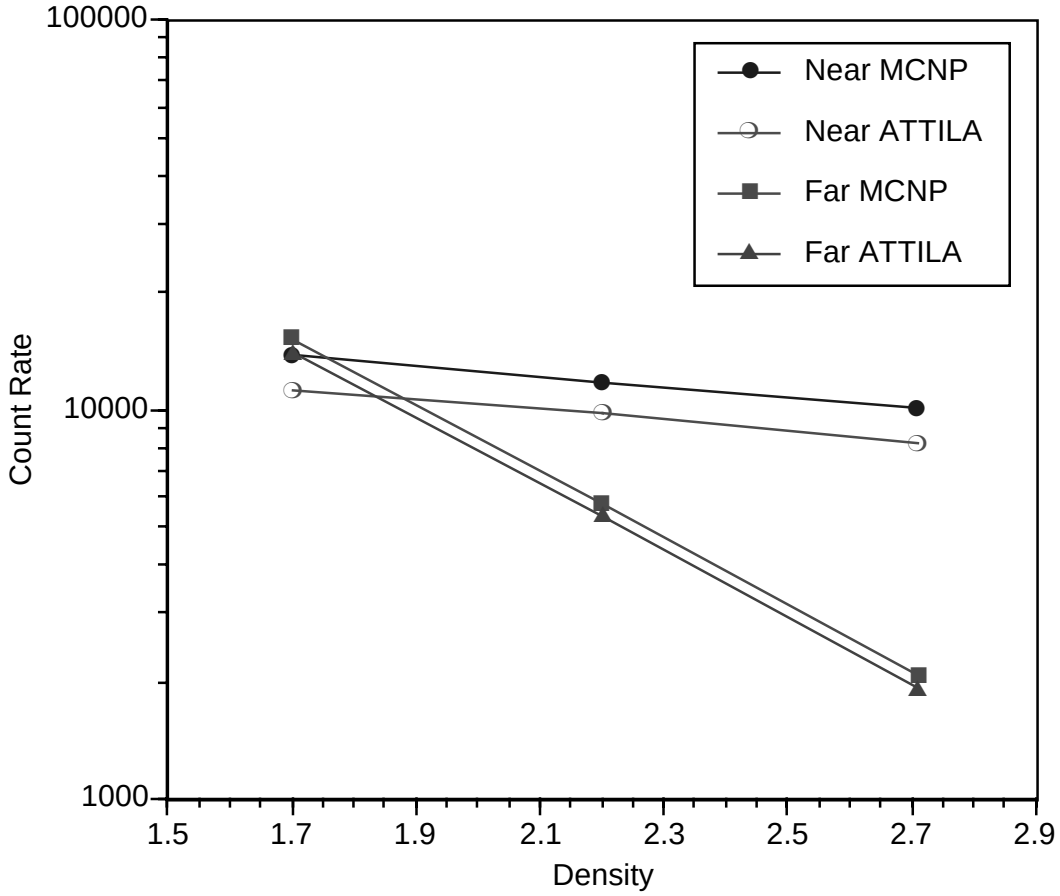

Figure 5: MCNP and ATTILA Count Rates Versus Density for Gamma Density Tool With Mudcake

C. Summary for Gamma-Ray Tool

Based upon the results in this section, it appears that ATTILA is very effective for gamma-ray density tools. Although the individual count rates differ from MCNP by as much as 19%, the slopes demonstrating the proportionality between the count rates and the density of the formation is in very good agreement, which is the final result needed by the well-logging industry. Possible differences in the count rates may arise from the multigroup cross sections, spatial error, and errors resulting from the last collided flux calculation (the bias quadrature set may not have enough angles in the solid angle associated with the near collimation hole). We note, that the results obtained without using the last collided flux for the near detector differ from MCNP by as much as 40-50%, demonstrating the necessity of using the last collided flux. Because of computer memory and time constraints, we have been unable to do a cross-section study and/or spatial error study.

VII. Conclusions

We have demonstrated that deterministic codes can be very effective and efficient for solving well-logging tool problems. Excellent agreement with Monte Carlo has been

obtained for both neutron porosity and gamma-ray density tools. We believe that ATTILA is the first deterministic code to effectively solve the gamma-ray density tools, especially the problem with mudcake. The most attractive feature of ATTILA is the ability to model the complex geometries that arise from these logging tools using an unstructured tetrahedral mesh. However, this is just a preliminary study. We have spent considerably more time in the developement of ATTILA than optimization and futher improvements can certainly be made.

The following is a list of potential areas of further study:

- Multigroup cross section improvement and the use of more groups
- Spatial mesh refinement study. ICEM CFD has a product that will refine the tetrahedral mesh in areas where steep gradients in the solution occur and coarsen the mesh where the gradients are small. This could lead to optimized meshes. Also, the implementation of p-adaptive refinement is an alternative to mesh refinement.
- Improvements in the first collision source.
- Improvements in the last collided flux methodology including better techniques and biased quadrature.
- Including time dependence capabilities. Adding time-dependence to ATTILA would allow for the modeling of the pulsed-neutron tools. Linear discontinuous differencing in time could be used leading to much greater accuracy than traditional time differencing based upon the diamond technique.
- Parallelization of ATTILA. This could lead to faster computational times.
- Improved MC biasing using ATTILA. We hope to eventually develop a MC/S_n version of ATTILA with true biased sampling rather than the simple weight window.

REFERENCES

1. J.J. ULLO, "Use of Multidimensional Transport Methodology on Nuclear Logging Problems," *Nucl. Sci. Eng*., **92**, 228 (1986).

2. T. A. WAREING, J.M. McGHEE and J.E. MOREL, "ATTILA: A Three-Dimensional, Unstructured Tetrahedral Mesh Discrete Ordinates Transport Code," *Trans Am. Nucl. Soc*., Washington D.C., Volume 75, pages 146-147 (1996).

3. T.A. WAREING, J.E. MOREL and D.K. PARSONS, "A First Collision Source Method for ATTILA, an Unstructured Tetrahedral Mesh Discrete-Ordinates Code," Proceedings ANS Radiation and Shielding Division Topical Conference, Nashville, Tennessee, Volume 1, pp. 376-382, April (1998).

4. L.J. LORENCE, Jr., J.E. MOREL, and G.D. Valdez, “User’s Guide to CEPXS/ONEDANT: A One-Dimensional Coupled Electron-Photon Discrete Ordinates Code Package,” Version 1.0, SAND89-1661 (1989).

5. “MCNP - A General Monte Carlo N-Particle Transport Code Version 4A,” J.F. BRIESMEISTER, Ed., LA-12625, Los Alamos National Lab. (1993).

6. Tom M. Evans and Todd A Wareing, “Tetrahedral Based Weight Windows for MCNP”, Los Alamos National Laboratory Memorandum, XTM: TME-97-210 (U), (1997).